A Refined Force Field for Molecular Simulation of Imidazolium-Based Ionic Liquids

Zhiping Liu, Shiping Huang, and Wenchuan Wang*

Division of Molecular and Materials Simulation, Key Lab for Nanomaterials, Ministry of Education, Beijing University of Chemical Technology, Beijing 100029, PR China

Received: April 14, 2004; In Final Form: June 17, 2004

An all-atom force field for a class of the room temperature ionic liquids of the 1-alkyl-3-methylimidazolium cation family was developed. The model is based on the AMBER force field with modifications on several parameters. The refinements include three aspects. (1) The force coefficients of the bond and angle parameters were adjusted to fit the vibrational frequency data, from both experiment and ab initio calculations. (2) The parameters for two types of torsions, which are absent in the original AMBER, were obtained by fitting the torsion energy profiles depending on dihedral angles. (3) The results of the minimum interaction energies and geometries for several ion pairs, calculated from ab initio and the force field, respectively, are compared. Then, the van der Waals (VDW) diameter of a type of hydrogen atom (H5) is adjusted. To validate the force field, we performed molecular dynamics (MD) simulations for five RTILs. The predicted densities are in better agreement than those reported from other simulations. The space distribution functions (SDFs) obtained from MD are visualized to depict the microscopic structures of these liquids. The internal energy components and the self-diffusion constants are also discussed.

1. Introduction

Room-temperature ionic liquids (RTILs) are a class of organic salts that remain liquid at or near room temperature.[1] Recently, RTILs have been attracting a great deal of attention of many researchers, as they have many potential applications in separations,[2,3] catalysis,[4,5] and electrochemistry.[6,7] These liquids are regarded as environmentally benign "green" solvents, because they are nonvolatile, thermally stable, and recyclable. Furthermore, through different combinations of cations and anions, there is a tremendous variety of "designer" solvents. With great versatility of their chemical and physical properties, ionic liquids can be thus tailored and tuned for specific tasks.[8]

Many research groups have reported the physical properties[9] for RTILs over large ranges of temperature and pressure, including melting points, densities, viscosities, solubilities, liquid−liquid phase equilibria, heat capacities, etc. The structures and dynamics of these liquids have also been studied by analytical techniques, such as X-ray diffraction, IR and Raman spectroscopy, NMR spectroscopy, neutron diffraction, etc. It is indubitable that our knowledge about these novel solvents has greatly increased recently. However, a significant barrier is the absence of understanding of how the chemical constituents and structures of RTILs affect their properties.

The first principle quantum chemistry (QM) calculation is a valuable technique to obtain useful information without any experiments. The method has been applied to RTILs to obtain the structures of ion pairs[10−12] and thermodynamic properties[11] in the ideal gas state. Unfortunately, QM calculations are very computation-intensive and can be only implemented in very small systems (typically, several tens of atoms). On the basis of the topology of molecules, some properties, such as melting point and toxicity, can be predicted by an empirical method, quantitative structure−property relation (QSPR).[13−15] However, the intrinsic relation between the microstructure and property cannot be revealed in this way.

Atomistic simulation, usually known as molecular simulation, is one of the most promising approaches to investigate structural and dynamic properties of molecules and materials.[16] Recently, several research groups reported the simulation results of a class of RTILs containing 1-alkyl-3-methylimidazolium (amim) cations by molecular dynamics (MD)[17−34] and Monte Carlo (MC)[35] methods. Thermodynamic properties of pure RTILs, such as density[17,18,26,33,35] (or molar volume), isothermal compressibility coefficient,[26,35] cohesive energy density,[26] the heat of vaporization,[25] and self-diffusion constant,[17,23,25,26,32] were compared with available experimental data. The microscopic structures of RTILs are depicted in simulations.[17,25,32,34] In addition, the results also indicate that the dynamical behavior of these liquids is similar to that of the supercooled liquids.[23,32]

The solvation structures of small molecules[18] and inorganic ions[28,29] in RTILs were studied through molecular dynamics. Attempts to calculate the properties related to the free energy[19,22] were also performed. Besides this, simulations efforts were extended to mixtures,[20] gas−liquid interfaces,[21] and the polarity,[31] characterized through the absorption spectrum of a solvatochromic molecule.

Success of molecular simulation for accurately predicting various properties depends on the quality of the inter- and intramolecular potential functions, i.e., the force fields. Several force fields, including AMBER,[36] CHARMM,[37] and OPLS[38] etc, have been developed and applied successfully in a variety of systems. However, limited researches on the force field specific for RTILs were reported in a systematical way.[33] The group of Lynden-Bell[17] developed both the all-atom and united-atom force fields, which were validated only by experimental crystal structures. Their force fields consist of the Buckingham potential and electrostatic interactions, and no intramolecular potentials are included. The Maginn group[26,27] reported molecular dynamics of [bmim][PF_6] (for abbreviations, see Figure 1) by a force field borrowed from CHARMM, but in a different way to obtain partial charges. They also used a rather simple united-atom model in MC simulations.[35] De Andrade et al.[24,25]

* To whom correspondence should be addressed. E-mail: wchwang@163bj.com

10.1021/jp048369o CCC: $27.50
Published on Web 08/04/2004

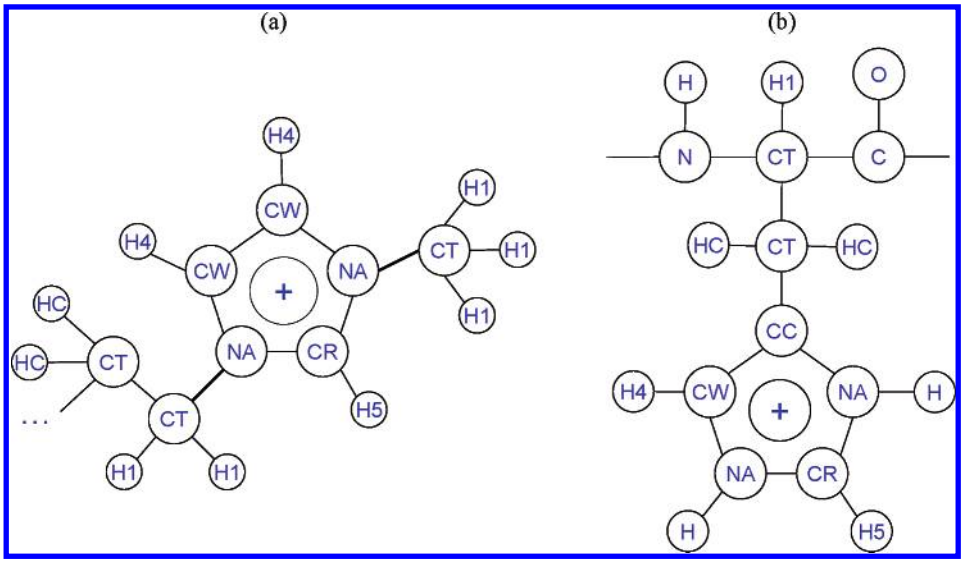

Figure 1. Schematic structure and atom type notations of (a) 1-alkyl-3-methylimidazolium cation (amim); (b) protonated histidine (HIP). Abbreviations used for 1-alkyl-3-methylimidazolium cations are mim = methylimidazolium, with prefixes a = alkyl, e = ethyl, b = butyl, and dmim refers to dimethylimidazolium. The nomenclature of the atoms is adopted from AMBER99 as follows: CR, sp^2 C in aromatic 5-menbered ring next to two nitrogens; CW, sp^2 C in aromatic 5-menbered ring next to carbon and NH; CC, sp^2 C in aromatic 5-menbered ring with one substituent and next to nitrogen; NA, sp^2 N in aromatic 5-menbered ring without lone pair; H4, H attached to aromatic carbon with one electronegative neighbors; H5, H attached to aromatic carbon with two electronegative neighbors; H1, H attached to aliphatic carbon with one electron withdrawing substituent; HC, H attached to aliphatic carbon without electron withdrawing substituent.

presented a force field mainly using the parametrization strategies from AMBER,[39] with the complement of two kinds of anions. Lopes et al.[33] proposed a model for a series of dialkylimidazolium cations based on the OPLS-AA/AMBER framework and discussed the parametrization by the torsion energy profiles in detail.

The aim of this work is to develop an all-atom force field for the 1-alkyl-3-methylimidazolium family RTILs, where the alkyl = methyl, ethyl, and butyl, in a systematical way. The cations include dmim, emim, and bmim (see definitions in Figure 1). The anions of interest are chloride (Cl^-), tetrafluoroborate (BF_4^-) and hexafluorophosphate (PF_6^-). This paper is organized as follows. In section 2, the parametrization strategy is described in brief. Then, a detailed analysis on each term of the force field is carried out. The molecular mechanics (MM) results from the force field proposed are compared with the crystallographic data from X-ray diffraction, vibrational frequencies from both experiment and QM, the torsion barrier energies and the minimum interaction energies and geometries of the ion pairs from QM. MD simulations are reported in section 3. In addition, the densities predicted by the force field and microscopic structures characterized by the radial distribution functions (RDFs) as well as the space distribution functions (SDFs), are compared with recent experimental results.[40,41] The components of the internal energies and self-diffusion constants are also discussed. Finally, some concluding remarks are addressed.

2. Force Field Development

The force field is expressed as the functional form in AMBER:[36]

$$E = \sum_{\text{bonds}} K_r(r - r_0)^2 + \sum_{\text{angles}} K_\theta(\theta - \theta_0)^2 + \sum_{\text{dihedrals}} \frac{K_\phi}{2}[1 + \cos(n\phi - \gamma)] + \sum_{i<j}\left[\frac{A_{ij}}{r_{ij}^{12}} - \frac{B_{ij}}{r_{ij}^{6}} + \frac{q_i q_j}{r_{ij}}\right] \quad (1)$$

The first three terms represent the bonded interactions, i.e., bonds, angles and torsions. The nonbonded interactions are described in the last term, including van der Waals (VDW, in the Lennard-Jones (LJ) 6−12 form) and Coulombic interactions of atom-centered point charges. Electrostatic and VDW interactions are calculated between only the atoms in different molecules or for the atoms in the same molecule separated by at least three bonds. The nonbonded interactions separated by exactly three bonds (1−4 interactions) are reduced by a scale factor, which is optimized[36] as 1/2 for VDW and 1/1.2 for electrostatic interactions. Here, the LJ 6−12 potential is written as

$$E_{\text{LJ}} = 4\epsilon_{ij}\left[\left(\frac{\sigma_{ij}}{r_{ij}}\right)^{12} - \left(\frac{\sigma_{ij}}{r_{ij}}\right)^{6}\right] = \epsilon_{ij}\left[\left(\frac{\sigma_{\text{min},ij}}{r_{ij}}\right)^{12} - 2\left(\frac{\sigma_{\text{min},ij}}{r_{ij}}\right)^{6}\right] \quad (2)$$

where ϵ_{ij} is the traditional well-depth. σ_{ij} and $\sigma_{\text{min},ij}$ are the distances between atoms i and j, at which the energy of the two atoms reaches zero and minimum, respectively. Obviously, $\sigma_{\text{min},ij} = \sqrt[6]{2}\sigma_{ij}$. Comparing eq 1 and eq 2, we get

$$A_{ij} = 4\epsilon_{ij}\sigma_{ij}^{12} = \epsilon_{ij}\sigma_{\text{min},ij}^{12}; \quad B_{ij} = 4\epsilon_{ij}\sigma_{ij}^{6} = 2\epsilon_{ij}\sigma_{\text{min},ij}^{6} \quad (3)$$

The LJ parameters for unlike atoms are obtained from the Lorentz−Berthelot (LB) combining rule

$$\epsilon_{ij} = \sqrt{\epsilon_{ii}\epsilon_{jj}}; \quad \sigma_{ij} = (\sigma_{ii} + \sigma_{jj})/2 \quad (4)$$

The parametrization procedures for the force field in this work are described as follows.

(1) Choose the atom type based on available force fields. The initial set of parameters (bonded and VDW) are deduced.

(2) Obtain optimized molecular geometry by performing QM calculations. The equilibrium bond lengths and angles are determined.

(3) Allocate charges to each atom center by fitting the ab initio electrostatic potential (ESP).

TABLE 1: Force Field Parameters for 1-Alkyl-3-methylimidazolium Cations, PF_6^- and BF_4^- Used in This Work

	nonbonded parameters					nonbonded parameters			
atom	ϵ_{ii} (kJ/mol)	σ_{ii} (Å)	q_i (e)	source	atom	ϵ_{ii}(kJ/mol)	σ_{ii} (Å)	q_i (e)	source
CR	0.3598	3.400	*a*	AMBER	HC	0.0657	2.650	*a*	AMBER
NA	0.7113	3.250	*a*	AMBER	P	0.8368	3.742	0.7562	AMBER
CW	0.3598	3.400	*a*	AMBER	B	0.3975	3.581	1.1504	ref 25
H4	0.0628	2.511	*a*	AMBER	F(PF_6^-)	0.2552	3.118	−0.2927	AMBER
H5	0.0628	1.782	*a*	this work	F(BF_4^-)	0.2552	3.118	−0.5376	AMBER
CT	0.4577	3.400	*a*	AMBER	Cl^-	0.6849	3.755	−1	fit to Tosi−Fumi[43]
H1	0.0657	2.471	*a*	AMBER					

bonds	r_0 (Å)	K_r (kJ mol^{-1} Å^2)	source	bonds	r_0 (Å)	K_r (kJ mol^{-1} Å^2)	source
CT−CT	1.526	1297	AMBER	CT−NA	1.472	1172	this work
CT−H1	1.080	1423	this work	CW−CW	1.343	1715	this work
CW−H4	1.070	1611	this work	CT−HC	1.090	1423	this work
CR−H5	1.070	1590	this work	P−F	1.600	795	this work
CR−NA	1.325	1674	this work	B−F	1.389	1213	ref 25
CW−NA	1.378	1506	this work				

angles	θ_0 (deg)	K_θ (kJ mol^{-1} rad^2)	source	angles	θ_0 (deg)	K_θ (kJ mol^{-1} rad^2)	source
CT−CT−CT	109.5	167	AMBER	CW−CW−NA	107.1	502	this work
CT−CT−H1	109.5	159	this work	CR−NA−CW	108.0	502	this work
CT−CT−HC	109.5	155	this work	NA−CR−NA	109.9	502	this work
CT−CT−NA	112.2	293	this work	H4−CW−NA	122.1	126	this work
H1−CT−H1	109.5	146	AMBER	H5−CR−NA	125.7	126	this work
HC−CT−HC	109.5	142	this work	CW−CW−H4	130.7	126	this work
H1−CT−NA	109.5	230	this work	F−P−F	90	335	this work
CW−NA−CT	125.7	209	this work	F−B−F	109.5	209	ref 25
CR−NA−CT	126.3	209	this work				

torsions	γ (deg)	K_φ/2 (kJ mol^{-1})	n	source	torsions	γ (deg)	K_φ/2 (kJ mol^{-1})	n	source
Proper Torsions									
NA−CR−NA−CW	180	50.21	2	this work	CT−CT−CT−H1	0	0.669	3	AMBER
NA−CR−NA−CT	180	8.368	2	this work	CT−CT−CT−CT	0	1.046	3	AMBER
H5−CR−NA−CW	180	6.276	2	this work	CT−CT−CT−HC	0	0.669	3	AMBER
H5−CR−NA−CT	180	6.276	2	this work	NA−CT−CT−CT	0	1.046	3	AMBER
CW−CW−NA−CR	180	50.21	2	this work	NA−CT−CT−HC	0	0.669	3	AMBER
CW−CW−NA−CT	180	8.368	2	this work	H1−CT−CT−HC	0	0.628	3	AMBER
H4−CW−NA−CR	180	8.368	2	this work	HC−CT−CT−HC	0	0.628	3	AMBER
H4−CW−NA−CT	180	6.276	2	this work	H1−CT−NA−CW	0	1.021	3	this work
NA−CW−CW−H4	180	6.276	2	this work	H1−CT−NA−CR	0	0.686	3	this work
NA−CW−CW−NA	180	50.21	2	this work	CT−CT−NA−CW	0	−0.745	1	this work
H4−CW−CW−H4	180	6.276	2	this work	CT−CT−NA−CR	0	−0.987	1	this work
Improper Torsions									
NA−NA−CR−H5	180	4.602	2	AMBER	CR−CW−NA−CT	180	8.368	2	this work
CW−NA−CW−H4	180	4.602	2	AMBER					

[a] The atom partial charges for cations are listed in Table 5.

(4) Adjust bond and angle force constants to fit the vibrational frequency data.

(5) Determine torsion parameters absent in step 1, by fitting the torsion energy profiles.

(6) Validate the force field using QM training sets, such as the minimum interaction energies and geometries of ion pairs. The VDW parameters are refined in this step. A new set of parameters are obtained.

(7) Return to step 4, since the vibrational frequencies are dependent on the parameters adjusted in step 5 and 6. Repeat step 5 and 6, until the deviations between the two sets of parameters are small enough.

(8) Validate the force field through liquid-phase simulation. Refine the parameters if necessary.

2.1. Atom Types and van der Waals Parameters. The assignments of the atom types of 1-alkyl-3-methylimidazolium (amim) cation are rather straightforward, because the imidazolium ring in amim exists in the protonated histidine (HIP), which is well-defined in AMBER, CHARMM, and OPLS. Therefore, the schematic structures and the atom notations in this work for both the amim cation and HIP are shown in Figure 1.

However, the VDW parameters in OPLS, AMBER, and CHARMM are quite different, especially for the ring H atoms. For example, the diameters of H5 (see Figure 1) are 1.247, 2.432, and 2.420 Å in CHARMM, AMBER, and OPLS, respectively. To determine which force field is more suitable for the ionic liquids, we performed molecular simulations for [bmim][PF_6] at 298 K and 1 bar (with the atom charges from section 2.4). The liquid densities obtained from OPLS, CHARMM, and AMBER in this work are 1.312, 1.453, and 1.331 g/cm^3, respectively. Compared with the experimental density of 1.3603,[42] AMBER is adopted in this work, since it gives a better fit than the others.

In summary, the strategies for obtaining atoms types and parameters (see Table 1) are as follows.

(1) The VDW parameters of cations are directly taken from AMBER99, and the diameter of H5 is adjusted in section 2.6.

(2) The force constant of bonds and angles and the coefficients of torsions are determined by a similar strategy in the literature.[25] If the parameter is not available, an analogous atom type is assigned to it. Here, the analogues of NA, CR, and CW are set to N*, CK, and CM, respectively. However, some of

TABLE 2: Bond Lengths for 1-Alkyl-3-methylimidazolium Cations from QM Calculations in This Work, and X-ray Diffraction Data

	bond lengths (Å)											
	calculated, this work[b] no. of carbons[c]			experimental data from X-ray diffractions no. of carbons[c]								
bond[a]	1	2	4	1[d]	2[e]	2[f]	4[g]	4[h]	12[i]	14[j]	16[k]	18[l]
CR−NA(m)	1.316	1.316	1.316	1.317	1.338	1.336	1.337	1.327	1.322	1.337	1.329	1.326
CR−NA(a)	1.316	1.315	1.315	1.315	1.297	1.326	1.332	1.332	1.326	1.330	1.327	1.321
NA-CW(m)	1.378	1.378	1.378	1.363	1.380	1.377	1.393	1.376	1.373	1.385	1.374	1.371
NA-CW(a)	1.378	1.378	1.378	1.377	1.387	1.371	1.369	1.379	1.374	1.389	1.384	1.370
CW−CW	1.343	1.343	1.343	1.330	1.319	1.338	1.345	1.350	1.334	1.343	1.342	1.336
NA-CT(m)	1.467	1.466	1.466	1.467	1.453	1.472	1.470		1.468	1.456	1.466	1.470
NA-CT(a)	1.467	1.478	1.478	1.469	1.490	1.481	1.485		1.477	1.462	1.469	1.471
data source				ref 46	ref 74	ref 75	ref 76	ref 77	ref 45	ref 78	ref 78	ref 47

[a] The letter in parentheses indicates that the bond is located close to the methyl (m) or alkyl (a) side. [b] The calculations were performed at the HF/6-31+G(d) level for the isolated ion. [c] This number refers to the number of carbons in the alkyl side chain. [d] In [dmim][PF_6]. [e] In [emim][$Ag(CN)_2$]. [f] In [emim][HF_2]. [g] In [bmim]Cl. [h] In [bmim][$B(C_6H_4(CF_3)$-4)$_4$]. [i] In [C_{12}mim][PF_6]. [j] In [C_{14}mim]Cl. [k] In [C_{16}mim]Cl. [l] In [C_{18}mim][PF_6].

these parameters are further adjusted to fit the vibrational frequencies in section 2.3.

(3) The VDW parameters of chloride are quite different from various force fields. As is suggested in the literature,[33] a set of parameters obtained by fitting the Tosi−Fumi[43] potential, which is developed for high-temperature molten salts, is adopted here.

2.2. Geometries of the Isolated Ions. The QM ab initio calculations were performed for the isolated ions by using the Gaussian 98[44] package at the RHF/6-31+G(d) level. After the molecular geometry was optimized, an additional vibrational analysis was followed to ensure the absence of negative frequencies and verify the existence of a true minimum. The minimum conformers here are in agreement with the former published ab initio results.[10,26,35,42] The most notable characteristic of the geometries of the amim cations is that the imidazolium ring preserves the planar geometry.

The bond lengths for the amim cations from our QM calculations are listed in Table 2, along with the X-ray experimental data for comparison. The results agree well with each other and are adopted in our force field (see Table 1).

As regards the anions, bond lengths of 1.609 Å for P−F in PF_6^- and 1.397 Å for B−F in BF_4^- are obtained by our QM calculations. In crystal, the PF_6^- exhibits slight asymmetry. Since the lengths of the six P−F bonds range from 1.58 to 1.61 Å,[45−47] an averaged value of 1.60 Å is adopted in our force field. In addition, the average B−F bond length of 1.389Å in BF_4^- is taken directly from the X-ray crystallographic data[48] in this work.

In summary, all the values of bond lengths and angles used in our force field are listed in Table 1.

2.3. Force Constants of Bonds and Angles. In general, once the geometry is obtained, the force constants can be adjusted by fitting vibrational frequencies to the model system. Because the IR and Raman frequencies data for RTILs are somewhat limited,[11,12,26,49,50] ab initio calculations are introduced here. However, the Hartree−Fock (HF) method overestimates the frequencies by approximately 10%.[51] Therefore, a scaling factor of 0.9 is suitable for HF calculations.[37]

In this work, molecular mechanics (MM) calculations were implemented with the TINKER package.[52] The MINIMIZE and VIBRATE modules were employed for the normal-mode analysis (NMA). The vibrational frequencies of a model system and the corresponding vibrational modes can be thus obtained. However, it is very difficult to find a global optimized set of the force constant parameters to fit all the frequencies, because the assignments of the frequencies have to be done manually. Here, we focused on the frequency of the ring stretching, which used to be overestimated significantly by AMBER.[25] The frequency calculated from the original AMBER is 1808 cm^{-1}, while the experimental value is 1574 cm^{-1}. The overestimation of the ring stretching frequency by AMBER was also reported from the group of Kollman.[53] For instance, the experimental frequency for benzene is 1596 cm^{-1}, compared with the predicted value of 1729 cm^{-1}. To improve the result, they reduced the force constants of one bond and two angles. In this work, we reduced the bond force constants related to the imidazolium ring and the angle force constants of H4−CW−NA, H4−CW−CW and H5−CR−NA. Consequently, an improved value of 1632 cm^{-1} was obtained. In contrast, the force constants of CR−NA-CW, CW−CW−NA and NA-CR−NA were increased to avoid other frequencies becoming too low. Some of the other parameters, such as those for torsions, were also adjusted to improve the results. The final set of parameters is listed in Table 1. For comparison, Table 3 shows the frequencies of bmim from QM, AMBER, this work, and the published experimental data.

In the case of anions BF_4^- and PF_6^-, it is impossible to fit the frequencies very well with only two force constants, bond and angle. The additional 1−3 interactions, i.e., Urey−Bradley (UB) terms, are introduced in CHARMM,[37] which leads to a better fit. However, for being consistent with AMBER, the UB interactions are not taken into account in this work. The frequencies for the anions are listed in Table 4.

2.4. Torsion Energy Barriers. There are no definitions for several dihedral angles in AMBER. The most important ones are those related to the bond NA−CT, which influence the rotation of the lateral chain. Four classes of torsions are missing here, including CR−NA−CT−H1, CW−NA−CT−H1, CR−NA−CT−CT and CW−NA−CT−CT. As is discussed in the literature,[33] the torsion parameters were not taken into account carefully in previous simulations of RTILs.[23,25,26]

In this work, the ab initio torsion energy profiles were obtained by using Gaussian 98 at the MP2/6-31+G(d)//HF/6-31+G(d) level. In the geometry optimization, all the degrees of freedom were allowed, except the dihedral angle of interest, which varied in a step of 10°. Although the basis sets here are smaller than those in the literature,[33] the results have been proven accurate enough.[39] Lopes et al.[33] applied a different optimization procedure under constraints. Instead, a simple and reasonable method was used here. In our method, the optimized conformers from QM at various dihedral angles were used directly in MM energy calculations by the ANALYZE module in TINKER.[52]

TABLE 3: Vibrational Wavenumbers (in cm^{-1}) for Bmim, Experimental Data and Calculated Values of QM, AMBER and This Work

	calculated					calculated			
IR[a]	QM[b]	this work	AMBER	form of vibration[c]	IR[a]	QM[b]	this work	AMBER	form of vibration[c]
3172	3144	3146	3074	CH ring str	1210	1211	1119	1252	CCH bend
3126	3127	3120	3066	CH ring str	1170	1154	1103	1221	CH ring bend
	3126	3142	3066	CH ring str		1135	1111	1053	Me NCH bend
	3022	3025	2982	Me(N) str	1114	1129	973	1107	CCH bend
	3016	3024	2980	Me(N) str		1105	1017	1091	CC alkyl str
	2987	3024	2989	CH_2(N) str	1094	1099	1072	1229	CH ring bend
2967	2954	2980	2981	Me(C) str		1076	1052	1029	Me NCH bend
2940	2941	2978	2984	CH_2 str	1028	1018	931	992	CC str
	2939	2953	2909	CH_2(N) str	1009	1009	927	917	complex bend
	2933	2909	2868	Me(N) str	989	994	909	902	ring i/p bend
	2920	2981	2981	CH_2 str	975	978	970	972	Bu CC str
	2896	2984	2978	CH_2 str	950	920	889	991	CCH bend
2878	2887	2906	2916	Me(C) str	880	911	882	828	CH ring o/p bend
	2883	2868	2868	CH_2 str		908	957	1156	CH ring o/p bend
	2875	2914	2905	CH_2 str		884	863	938	Bu CC str
1575	**1588**	**1632**	**1808**	ring str	780	776	777	870	CCH bend
	1583	1641	1813	ring str	752	773	717	812	complex bend
	1487	1384	1451	CH_2 bend		713	725	812	CCH bend
1467	1482	1442	1392	Me(N) bend	698	704	689	664	complex bend
	1477	1498	1437	CH_2 bend	651	641	630	595	ring o/p bend
	1474	1386	1422	Me(C) bend		614	588	497	ring o/p bend
	1467	1436	1494	CH_2 bend	600	602	563	553	ring o/p bend
	1466	1420	1459	CH_2 bend	417	422	411	396	alkyl i/p bend
1431	1459	1424	1398	Me(N) bend		387	449	512	alkyl i/p bend
	1439	1536	1527	Me(N) bend		303	252	282	alkyl o/p bend
	1422	1405	1507	ring str		261	299	331	complex bend
1387	1412	1376	1410	Me(C) bend		238	278	242	CCC bend
	1400	1555	1659	CCH bend		231	240	256	Me(C) tors
	1379	1485	1696	ring str		191	203	185	complex bend
1340	1363	1334	1558	CCH bend		110	127	124	Et tors
	1315	1176	1282	CH ring bend		91	49	20	Me(N) tors
1301	1309	1240	1314	CCH bend		75	89	76	complex bend
	1294	1272	1298	CCH bend		69	79	79	Pr tors
1284	1280	1198	1400	CCH bend		32	30	26	Bu tors
	1272	1144	1448	CCH bend					

[a] From the literature.[11] [b] QM was performed at HF/6-31+G(d) level and a scaled factor of 0.9 is applied. [c] Mainly from the literature;[11] Note that Me, Et, Pr, and Bu refer to methyl, ethyl, propyl and butyl, respectively; i/p bend is in-plane bending; o/p bend is out-of-plane bending; tors is torsion; str is stretching.

TABLE 4: Calculated and Experimental Vibrational Wavenumbers (in cm^{-1}) for PF_6^- and BF_4^-, Experimental Data and Calculated Values of QM and from This Work

PF_6^-			BF_4^-		
	calculated			calculated	
IR[a]	QM[b]	this work	IR[c]	QM[b]	this work
	293	394		331	309
471	445	394		490	358
558	537	446		720	600
	556	486	1052	1031	1199
	713	486			
838	857	929			

[a] From the literature;[11] [b] QM is performed at the HF/6-31+G(d) level and a scaled factor of 0.9 is applied. [c] From the literature.[71]

Finally, the coefficients of the four types of dihedrals were optimized to fit the QM torsion energy profiles for dmim and emim.

The optimized parameters in this work are listed in Table 1. The energy profiles from QM and MM calculations are shown in Figure 2. As is seen, our results are in fair agreement with those of Lopes et al.,[33] although the torsion energy barriers in this work are systematically larger. For example, the energy barrier of CW−NA−CT−H1 is 3.6 kJ mol^{-1} in this work, while it is about 2 kJ mol^{-1} in the literature.[33] This disparity could result from the different basis sets in ab initio calculations.

Lopes et al. [33] also obtained the coefficients for NA−CT−CT−CT, which are very close to that of CT−CT−CT−CT (see Table 3 in the literature[33]). Therefore, the coefficients of CT−CT−CT−CT in AMBER were simply used for NA−CT−CT−CT in this work.

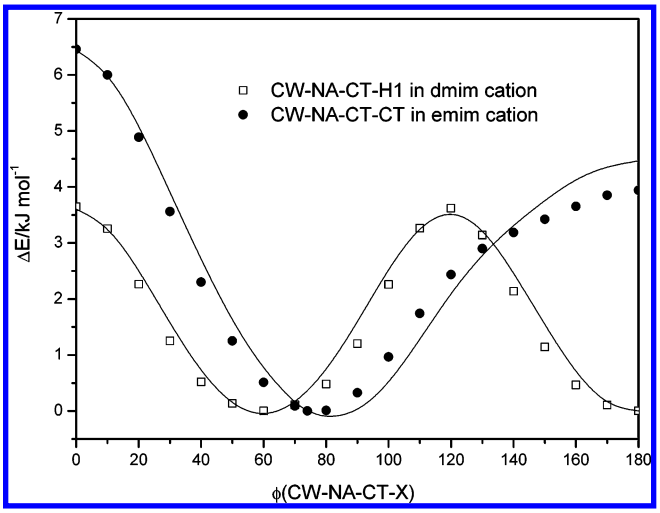

Figure 2. Torsion profiles of the dihedrals involving the NA−CT bond in dmim and emim cations, calculated by QM (dots) and MM (lines) in this work.

2.5. Atom Charges. The method to determine atom charges used in AMBER, known as restraint electrostatic potential (RESP) fit,[54] is proven[36,39,55−57] to be very efficient and successful for a variety of systems. In CHARMM,[37] TIP3P water

TABLE 5: Partial Charge on Each Atom of 1-Alkyl-3-methylimidazolium Cations from RESP Fitting from This Work

	q_i/e		
atom[a]	dmim	emim	bmim
CR	−0.0083	0.0213	−0.0055
NA(m)	0.0591	0.0618	0.0596
NA(a)	0.0591	0.0095	0.0682
CW(m)	−0.1705	−0.1353	−0.1426
CW(a)	−0.1705	−0.2094	−0.2183
H5	0.2329	0.2189	0.2258
H4(m)	0.2476	0.2320	0.2340
H4(a)	0.2476	0.2616	0.2633
CT(m)	−0.0740	−0.0808	−0.0846
H1	0.1085	0.1076	0.1085
CT(a1)	−0.0740	0.0234	−0.0153
H1	0.1085	0.0906	0.0796
CT(a2)		−0.0531	0.0107
HC		0.0487	0.0204
CT(a3)			0.0309
HC			0.0157
CT(a4)			−0.0713
HC			0.0294
	dipole moment (D)		
	dmim	emim	bmim
RESP	1.0276	1.8746	5.9166
QM	1.0250	1.8400	5.8970

[a] The letter in parentheses indicates that the atom is located close to the methyl (m) or alkyl (a) side.

is used as a "probe" molecule, and then the minimum interaction energies and geometries between water and the model molecules are determined to fit its charges. In contrast, the charges are obtained through an empirical way in OPLS. Several MC simulations are thus required to attain the best fit to condensed-phase experimental properties. Both approaches are not as convenient as RESP.

In this work, the one-conformation two-step RESP method was used to derive the atom charges by fitting the electrostatic potential generated from QM calculations at HF/6-31G+(d) level. The results in Table 5 indicate that the dipole moments from the QM calculations (see the last row in Table 5) are well reproduced with the RESP charges. In contrast to the geometries of the imidazolium ring, the charge distribution is not symmetric. The charge on CW near the alkyl side is about 50% larger than that on CW near the methyl side for both emim and bmim. It is also found that at the end of the alkyl chain, the total charge on the methyl group is nearly zero. This feature indicates that if more carbons are added to the alkyl chain, it is reasonable to set the charges on these carbon atoms to zero, for avoiding the computation-intensive QM calculations.

For consistency, different authors,[17,25,26,33,34] including this work, used their own charge distributions. However, further evaluation of the charge distribution relies on the energy-related experimental data, such as the heats of vaporization, free energies of hydration, which are often used in the development of force field.

2.6. Geometries and Interaction Energies of Ion Pairs. Because of the availability of high-quality ab initio calculations, the properties of the molecule complexes (or supermolecules) are extensively used in the parametrizations and calibrations of force fields.[58,59] In the development of a classical force field, the most frequently used complexes are the molecular dimers, and the clusters of model compounds and water.[37,60,61] In such a procedure, the minimum geometries and interaction energies of the complex of interest are determined by ab initio calculations (QM) and subsequently compared with the results of the force field (MM). In this work, the properties of the ion pairs were employed to validate the force field proposed.

TABLE 6: Interaction Energy and C−H···F Distances of Ion Pairs Optimized by QM, AMBER, and This Work

ion pair	energy (kJ mol^{-1})	distance[b] (Å)
[dmim][PF_6]		
QM[a]	−323.5	2.55/2.09/2.64/2.33/2.54
AMBER	−321.6	2.84/2.46/3.05/2.46/2.84
this work	−326.1	2.67/2.17/2.75/2.23/2.75
[emim][BF_4]		
QM[a]	−345.6	2.44/2.11/2.71/2.33/2.69/2.64
AMBER	−344.0	2.69/2.44/3.02/2.40/2.71/2.65
this work	−350.7	2.59/2.19/2.74/2.17/2.66/2.68
[bmim][PF_6]		
QM[a]	−320.8	2.44/2.20/2.59/2.24/2.60/2.76
QM[c]	−341.3	2.40/2.13/2.48/2.15/2.52/2.68
AMBER	−319.1	2.74/2.44/2.93/2.40/2.70/2.66
this work	−324.3	2.62/2.19/2.63/2.16/2.66/2.68

[a] The QM calculations are performed at the HF/6-31+G(d) level in this work. [b] The distances are listed in the left-to-right sequence (see Figure 3). [c] The data are extracted from the literature,[11] in which the QM calculations are performed at the HF/6-31G(d) level.

The lowest energy structures of the three types of ion pairs, [dmim][PF_6], [emim][BF_4], and [bmim][PF_6], were obtained by the ab initio calculations at HF/6-31+G(d) level without any constraints on the degrees of freedom, as is shown in Figure 3, parts a−c, respectively. Generally, if the distance between the H atom in a cation and the F atom in an anion (C−H···F) is less than 2.70 Å, the interaction is recognized as hydrogen bonding.[62] Therefore, these distances are labeled in Figure 3 and listed in Table 6. The interaction energies of the complexes are also listed in Table 6.

As is seen in Figure 3a, the geometry of the ion pair [dmim]-[PF_6] calculated from QM is asymmetric, which is contrary to the cation and the anion. PF_6^- tends to decrease the total energy of the system by rotating and tilting. However, in the case of MM, the asymmetry disappears and the lengths of the hydrogen bond are significantly larger than those from QM. For example, QM gives the shortest distance of C−H···F of 2.09 Å, while it is 2.46 Å in MM. As the VDW diameter of H5 decreases, the asymmetry emerges again. From our calculations, when r_{min} ($r_{min} = \sigma_{min}/2$) of H5 is less than 1.2 Å, the asymmetry appears. By further calculations, we obtained an optimized r_{min} of 1.0 Å, which gives 2.17 Å for the shortest distance of C−H···F. In addition, the geometries from MM are very close to those from QM (see Table 6).

The results for the other two ion pairs, [emim][BF_4] and [bmim][PF_6], are consistent with those of [dmim][PF_6]. The distances of C−H···F are notably overestimated by MM. The discrepancies between the QM and MM are reduced when the VDW diameter of H5 decreases. It is corroborated that a value of 1.0 Å is suitable for the r_{min} of H5, which is therefore adopted in our force field.

As is seen in Table 6, the interaction energies of the ion pairs from MM are generally smaller than those from QM without additional adjustment of the VDW diameter of H5. After the adjustment, the energies become too large. However, the QM calculation is dependent on the method and the basis sets. For example, the interaction energies at the HF/6-31G(d) level and the MP2/6-31+G//HF/6-31G(d) level for [bmim][PF_6] are −341.3 and −369.9 kJ mol^{-1}, respectively,[11] while it is −320.8 kJ mol^{-1} at the HF/6-31+G(d) level in this work. It is also noticed that the distances of C−H···F are not sensitive to the

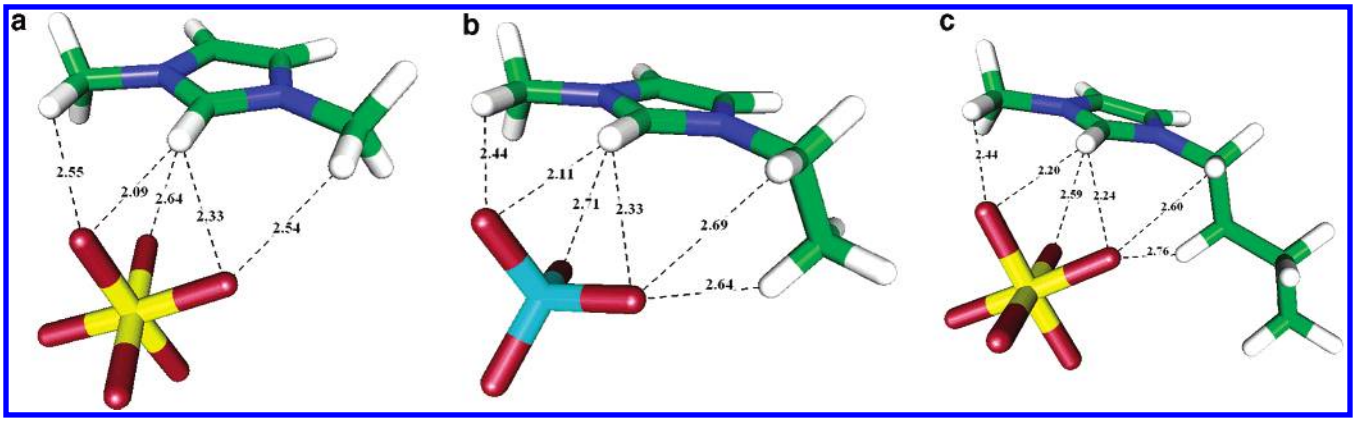

Figure 3. (a) Structure of [dmim][PF_6] ion pair with minimum energy optimized by QM calculations at HF/6-31+G(d) level, this work. (b) Structure of [emim][BF_4] ion pair with minimum energy optimized by QM calculations at HF/6-31+G(d) level, this work. (c) Structure of [bmim]-[PF_6] ion pair with minimum energy optimized by QM calculations at HF/6-31+G(d) level, this work.

basis sets in the QM calculations. For reference, the values from the literature[11] are also listed in Table 6.

3. Molecular Dynamics Simulations

3.1. Simulation Details. Liquid-phase simulations were performed in this work by using the molecular dynamics package MDynaMix[63] for RTILs [dmim]Cl, [dmim][PF_6], [emim][BF_4], [bmim][BF_4], and [bmim][PF_6] with the standard periodical boundary conditions. The system consists of 128 ion pairs, containing several thousands of atoms. An additional simulation of 192 ion pairs was also carried out for [dmim]-[PF_6], and almost the same results (RDF, internal energies, and self-diffusion constants) were obtained. As is suggested in the literature,[63] our simulations started from an fcc lattice at a very low density. After the system was relaxed in the *NVE* ensemble for a few MD steps (typically a few hundred steps) to reduce the possible overlapping in the initial configuration, the density could be gradually increased to a reasonable value. The simulation was then performed in the Nose-Hoover[64] *NpT* ensemble with coupling constants 700 and 30 fs. Each simulation was equilibrated for at least 200 ps until a steady-state was reached. The multiple time-step algorithm[65] was adopted in this work. The long and short time steps were 2 and 0.2 fs, respectively. The production phase persisted 100 ps, in which the trajectories were dumped in an interval of 10 fs for further analysis. Both the dispersion and Coulombic interactions were cut off at a radius of 15 Å, and the Ewald summation[66] was implemented for the latter.

3.2. Liquid Densities. Despite the fact that the database of RTILs expands quickly, limited data can be used to validate a proposed force field. One of the available sources is liquid density. However, it is noticed that sometimes trace amounts of impurities such as water, chloride, and sodium ions in RTILs could change the value of the density dramatically.[67] In this work, experimental data and the simulated densities from the literature are compared with our results. As is shown in Table 7, the predicted densities from our force field are in good agreement with the experimental data. The results are also consistent with the simulations from other authors. Generally, the densities of RTILs are underestimated with a force field based on AMBER.[25,28,33] For example, the predicted values from the AMBER based force fields are 1.337[33] and 1.33,[28] while our result is 1.350, against the experimental density of [bmim]-[PF_6],[42] 1.360 g cm^{-3}. It is noted that, in our simulations, the density is not sensitive to the charge distribution of both ions. Consequently, the improvement of the density calculated in this work over the densities predicted by the other AMBER based force fields is attributed to a reasonable adjustment of the VDW diameter of the H5 atom.

TABLE 7: Liquid Phase Densities of Ionic Liquids from This Work, Literatures, and Experiments

		densities (in g/cm^3)			
		simulation			
RTIL	*T* (K)	this work	lit.[a]	exptl	source
[dmim][PF_6]	400	1.459	1.49[b] [17]		
[bmim][PF_6]	298	1.350	1.337 [33], 1.368 [26] 1.33 [28]	1.360	ref 42
[bmim][PF_6]	313	1.338		1.349	ref 42
[bmim][PF_6]	333	1.318		1.332	ref 42
[emim][BF_4]	298	1.284	1.255 [25]	1.279	ref 79
[emim][BF_4]	313	1.266		1.266	ref 79
[bmim][BF_4]	298	1.194	1.174 [25]	1.211	ref 67
[dmim]Cl	423	1.150	1.06 [17], 1.16[b][17]	1.138	ref 80

[a] The number in the square bracket refers to the literature source. [b] United-atom model.

3.3. Components of Potential Energy. Table 8 presents a breakdown of the potential energy into LJ, electrostatic, and bonded interaction energies. The first two terms are further divided into intermolecular (1−4 interacions) and intermolecular parts. The bonded interactions include bond stretching, angle bending and torsion terms. As is seen in Table 8, the electrostatic interactions, which are four times as large as the VDW interactions, contribute the main part of the total potential energy. It reflects the "ionic feature" of these liquids.

It is observed that the LJ contribution increases with the length of the alkyl chain and decreases with the increase of temperature, as is expected. The electrostatic contribution is not sensitive to temperature, because the LJ potential varies with the distance more sharply than the Coulombic interaction.

It is interesting to notice that the intramolecular part of the LJ interaction changes its sign as the number of carbons in the alkyl chain increases. It is of a negative value for dmim salts, and still negative but of a smaller value for emim salts. However, it becomes positive for bmim salts. Because the LJ 1−4 interactions of the ring are evidently negative, the positive energies must be contributed by the side chain. In the gas phase (i.e., isolated ion pair, see Figure 3), the trans-conformation of the alkyl chain is the most stable one, which cannot contribute a positive 1−4 LJ energy. It indicates that the conformation of the alkyl chain in the condensed liquid phase is quite different from that in the gas phase.

Both the heats of vaporization, ΔH^{vap}, and the cohesive energy densities, *c*, are related to the change in internal energy, ΔU^{vap},

TABLE 8: Potential Energy Contributions of Various Terms from Molecular Dynamics Simulations from This Work

		potential energies (in kJ mol^{-1})									
		LJ			electrostatic			bonded			
RTIL	T (K)	total	intra	inter	total	intra	inter	total	bond	angle	torsion
[dmim][PF_6]	400	−53.8	−1.5	−52.3	−300.7	137.2	−436.1	100.6	35.8	43.7	21.2
[bmim][PF_6]	298	−71.3	1.5	−72.8	−284.6	145.5	−421.0	108.0	38.4	50.8	18.8
[bmim][PF_6]	313	−70.4	1.6	−71.9	−284.4	145.6	−420.5	113.4	40.6	53.4	19.4
[bmim][PF_6]	333	−68.0	1.8	−69.7	−286.0	145.6	−419.2	119.8	42.9	56.6	20.3
[emim][BF_4]	298	−54.9	−1.1	−53.8	−289.8	160.0	−455.8	78.4	28.3	33.9	16.1
[emim][BF_4]	313	−53.7	−1.2	−52.5	−290.4	159.2	−454.5	82.0	29.7	35.7	16.6
[bmim][BF_4]	298	−61.9	1.5	−63.4	−312.8	145.6	−443.4	101.1	36.1	46.3	18.7
[dmim]Cl	423	−28.3	−1.4	−26.9	−393.8	137.3	−526.5	79.3	27.2	30.4	21.7

TABLE 9: Intermolecular Potential Energy (U^{int}), the Heat of Vaporization (ΔH^{vap}), Molar Volume (V_m), and Cohesive Energies Density (c) from Molecular Dynamics Simulation from This work

RTIL	T (K)	U^{int} (kJ mol^{-1})	ΔH^{vap} (kJ mol^{-1})	V_m (cm^3 mol^{-1})	c (J cm^{-3})
[dmim][PF_6]	400	−488.4	165.6	165.9	978.1
[bmim][PF_6]	298	−493.8	172.0	210.5	805.5
[bmim][PF_6]	313	−492.4	170.7	212.4	791.6
[bmim][PF_6]	333	−488.9	167.4	215.6	763.6
[emim][BF_4]	298	−509.6	161.3	154.2	1030
[emim][BF_4]	313	−507.0	158.9	156.3	1000
[bmim][BF_4]	298	−506.8	161.8	190.0	838.3
[dmim]Cl	423	−553.4	187.1	115.3	1593

from liquid to gas phase, defined as

$$\Delta H^{vap} = \Delta U^{vap} + RT, \quad c = \Delta U^{vap}/V_m \tag{5}$$

where R is the gas constant and V_m is the molar volume of the liquid. By definition

$$\Delta U^{vap} = U(\text{vap}) - U(\text{liq}) \tag{6}$$

where U(vap) and U(liq) are the total potential energies in the vapor and liquid phase, respectively. It is stressed that in the simulation the cations and anions are treated as two species, while in eq 6 they are considered as one species, i.e., an ion pair. ΔU^{vap} can be calculated through the thermodynamic routes as

$$\begin{array}{ccc} \text{AB(liq)} & \xrightarrow{\Delta U^{vap}} & AB\text{(vap)} \\ \downarrow \Delta U_1 & & \uparrow \Delta U_3 \end{array}$$

$$\text{A}^+\text{(ig)} + \text{B}^-\text{(ig)} \xrightarrow{\Delta U_2} \text{AB(ig)} \tag{7}$$

where ig represents ideal gas and AB indicates the ion pair. Although the conformations of the ions in the liquid and ideal gas states are not the same, it is a reasonable approximation that the changes of intramolecular energies between the two states can be ignored. Therefore, ΔU_1 is just the intermolecular energies of the liquid, U^{int}, which can be extracted from the simulation. ΔU_2 is the interaction energies of the ion pair, $U^{ion\ pair}$, which is discussed in section 2.6 (see Table 6). Obviously, ΔU_3 can also be ignored. Thus,

$$\Delta U^{vap} = U^{ion\ pair} - U^{int} \tag{8}$$

The intermolecular energies, heats of vaporization, molar volumes, and cohesive energy densities are summarized in Table 9. The cohesive energy density of [bmim][PF_6] at 298 K is 849 J/cm^3, which is in fair agreement with the reported value of 791 J/cm^3 by Morrow and Maginn.[26] As is seen in Table 9, RTILs have extremely high value of the heats of vaporization and the cohesive energy densities, leading to a negligible vapor pressure. It suggests that in contrast to the volatile organic compounds (VOCs), RTILs are considered as a kind of environment-friendly solvents. Generally, the smaller the ion, the larger the cohesive energy density. The sequence is dmim > emim > bmim and Cl^- > BF_4^- > PF_6^-. This is due to the closer packing in smaller RTILs.

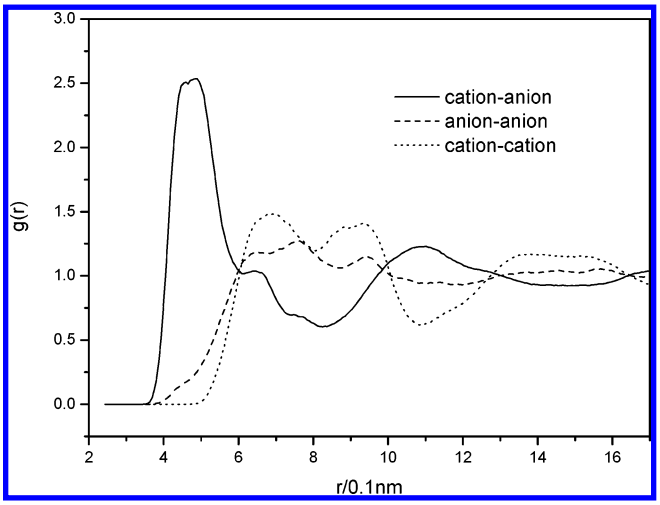

Figure 4. Center of mass radial distribution functions of [bmim][PF_6] at 298 K and 1 bar.

3.4. Microscopic Structures. The center-of-mass radial distribution functions (RDFs) for the cation−anion, anion−anion, and cation−cation were computed for the RTILs of interest. The RDFs of the same RTIL at different temperatures are almost the same, because the temperature range considered in this work is within 40 K, being too small to induce variation in the RDFs. The RDFs of different RTILs are also very similar. Therefore, for illustration, only the RDFs of [bmim][PF_6] at 298 K and 1 bar are shown in Figure 4. It is observed that the oscillations of the RDFs span beyond 17 Å, which is about a half of the length of the simulation box. The charge ordering is the characteristic of a system dominated by the long-range Coulombic interactions. According to the RDF of the cation−anion, two solvation shells are found located at 4.8 and 11.0 Å, respectively. Morrow and Margin[26] reported three solvation shell locations at 4.3, 10.6, and 17.6 Å, which are slightly smaller than the values in this work. The third shell is not observed because the length is beyond our simulation box. The locations of the maximum and minimum in the cation−anion RDFs of RTILs are listed in Table 10, as well as the coordination numbers for the first solvation shell. The coordination number, N, is calculated via the integral of RDF from zero to the first minimum

$$N = 4\pi \int_0^{R_{min1}} \rho g(r) r^2 \, dr \tag{9}$$

TABLE 10: Maximum and Minimum Positions of Center of Mass Radial Distribution Functions for Cation−Anion of Ionic Liquids and the First Shell Coordination Numbers from This Work

RTIL	positions[a] (Å) R_{max1}	R_{min1}	R_{max2}	coordination nos.
[emim][BF_4]	4.3	7.4	10.5	7.1
[bmim][BF_4]	4.4	7.6	11.6	6.1
[bmim][PF_6]	4.8	8.2	11.0	6.5
[dmim][PF_6]	4.7	7.6	10.6	7.2
[dmim]Cl	4.3	6.5	9.8	6.7

[a] The values in this column refer to the locations of the maximum and minimum of the RDF.

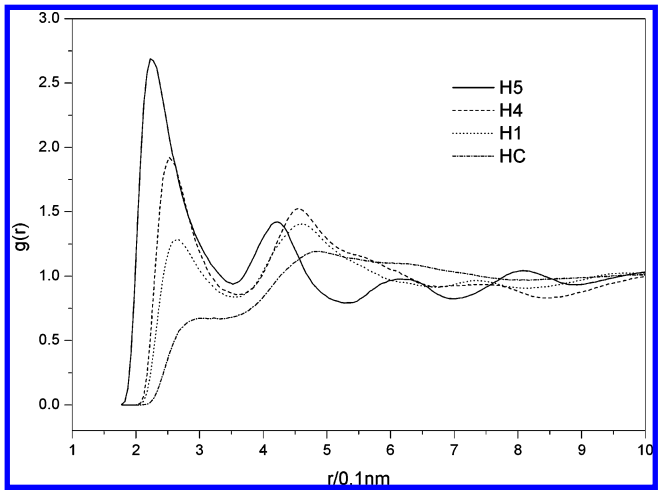

Figure 5. Site−site radial distribution functions between various kinds of H atoms in the bmim and F atom in PF_6^- at 298 K and 1 bar. For the notations, see Figure 1.

where ρ is the number density and R_{min1} refers to the first minimum in $g(r)$. As is seen from Table 10, there are about six to seven counterions surrounding each ion.

A more detailed liquid structure can be desrcibed by the site−site pair RDFs. Figure 5 shows the RDFs for the fluorine atom in PF_6^- and different hydrogen atoms of the bmim. It is found that the F atom prefers to distribute around H5, rather than H4 and H in the methyl (H1) or butyl group (HC). The first maximum locations of the RDFs are 2.23, 2.53, and 2.70 Å for H5, H4, and H1, respectively, and no pronouced ordering is found between the F atom and the HC at the end of the butyl group. These RDFs indicate the order of activities of the different H atoms in the cation, H5 > H4 > H1 > HC.

The activity of the same kind of H atom also varies with the RTILs. The RDFs of H5−X (X = F, Cl) in different RTILs are shown in Figure 6. The RDF of H5−Cl in [dmim]Cl presents an obvious higher peak than others. It is also found that the interaction between H5 and BF_4^- is more intimate than that with PF_6^-. This observation is consistent with the experimental data of NMR chemical shift[68] and the fact that the BF_4^- salts with short alkyl chain ($n < 6$) is miscible with water,[9] while a two phase mixture forms with the PF_6^- salts and water.[69] The first peaks occur at 2.18 and 2.23 Å for ionic liquids with anions of BF_4^- and PF_6^- respectively. Although the topic remains controversial[62,68,70−72] on the presence or absence of C−H···F hydrogen bonding between the imidazolium cation and the anions of BF_4^- and PF_6^-, it is revealed by our simulation that the interaction between the H5 and the X atom decreases in the order Cl^- > BF_4^- > PF_6^-. The RDFs of H4−X and H1−X are not demonstrated here for they are very similar to that of H5−X.

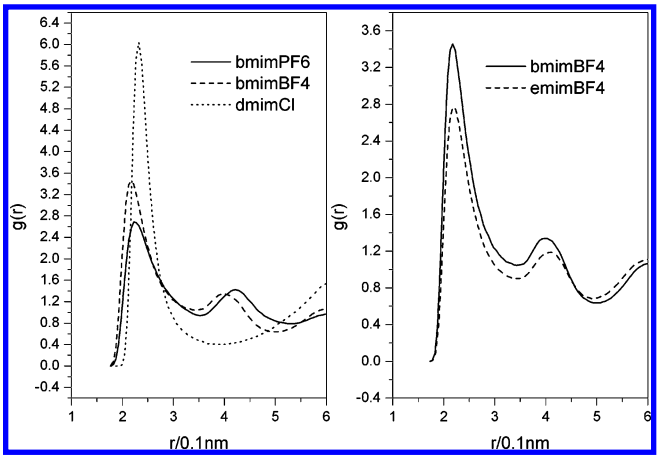

Figure 6. Site-site radial distribution functions between H5 in the imidazolium ring and X (X = F, Cl) atom in the anion for various ionic liquids at 298 K and 1 bar.

The liquid structure can be depicted by a more intuitive method, i.e., the space distribution functions (SDFs). SDF gives the probability of finding an atom in the three-dimensional space around a center molecule, in contrast to the average values given by RDF. In this work the SDFs are visualized by the software package gOpenMol.[73] As is see in Figure 7, the probability distributions of the Cl^- and PF_6^- around the dmim cation are similar but with different characteristics. There are mainly three high probability regions where the counterions are found, which contribute to the first shell in the RDF (see Figure 4 for reference). Not surprisingly, the largest density is around the CR, both above and below the plane of the imidazolium ring, since it is the region of highest positive charge. The other two regions are between the CW−H4 and the methyl group. With two anions in each region, there are six counterions can be found in the first shell. In additional, a much smaller region exists between the two CW−H4 groups. The result agrees well with the calculated coordination number of six to seven given in Table 10. In addition, the two regions along with the NA−CT bond represent the second shell in the RDF (see Figure 7).

Hanke et al.[17] also reported three-dimensional probability distributions of [dmim]Cl and [dmim][PF_6] by molecular simulations. The results are very similar to this work, except that they obtained a much larger region between the two CW−H4 groups (see Figure 2 in the literature[17]). There are thus mainly four regions in their simulation, instead of three in this work. More recently, Hardacre et al.[40,41] studied the liquid structure of the two ionic liquids by neutron diffraction experiments combined with an empirical potential structure refinement (EPSR) process. From their result, the region between the two CW−H4 groups does not exist (see Figure 5a in the literature[41]). Therefore, the force field proposed in this work is more reasonable than that used in the literature.[17]

A pronounced difference between the distribution of the Cl^- and PF_6^- anions in dmim salts is that the highest density (see the orange contour which refers to 20 time average density) exists in the three regions in [dmim]Cl, while it exists only in the region around the CR in [dmim][PF_6]. The other difference is that the highest density region shifts toward the ring as the anion changes from Cl^- to PF_6^-, mainly due to the size of the anion. It is consistent with the results from EPSR[41] and reported by recent simulations.[34]

Figure 8a shows the effect of the length of the alkyl chain on the distribution of the anions around the cations. In [bmim]-[PF_6], the butyl group pushes the region around the CR toward the methyl side. On the contrary, the smaller region between

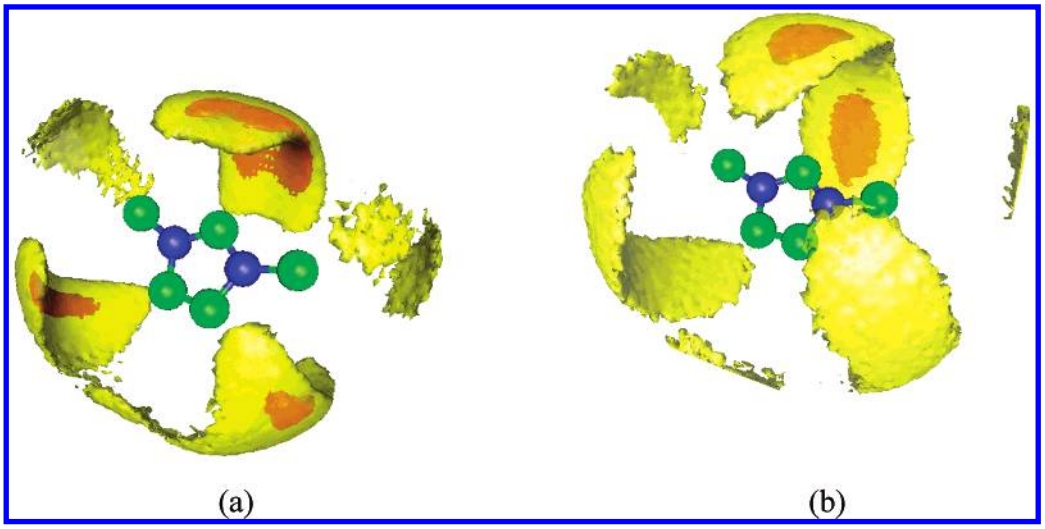

Figure 7. Three-dimensional probability distributions of (a) Cl^- around dmim and (b) PF_6^- around dmim from molecular simulations in this work. In each case, the orange and yellow bounded contour surfaces are drawn at 20 and 6 times the average density, respectively.

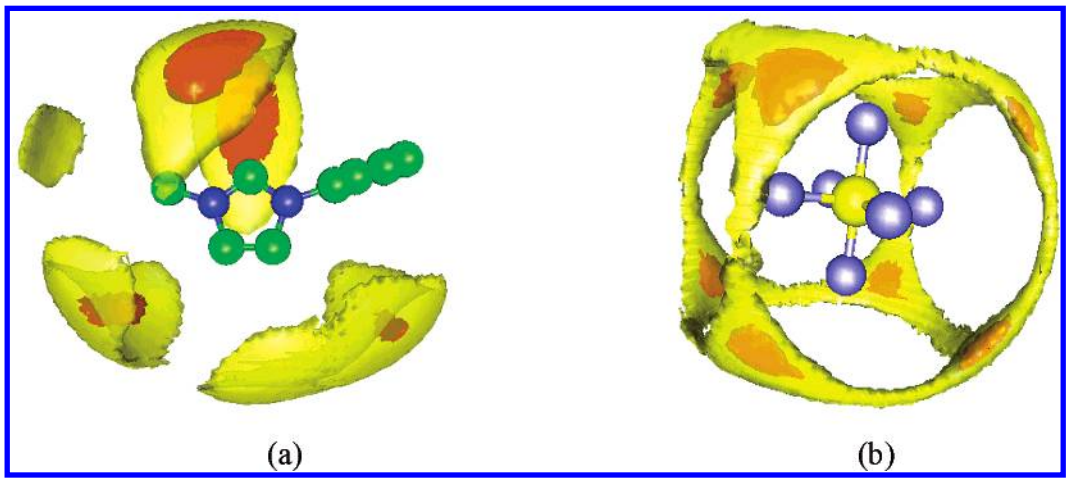

Figure 8. Three-dimensional probability distributions of (a) PF_6^- around bmim and (b) CR in bmim around PF_6^- from molecular simulations in this work. For part a, the orange and yellow bounded contour surfaces are drawn at 20 and 6 times the average density, respectively. For part b, the orange and yellow bounded contour surfaces are drawn at 3 and 2 times the average density, respectively.

the two CW−H4 groups grows and shifts toward the butyl side. In addition, a well-ordered distribution of the CR in the bmim cation around the PF_6^- anion is found (see Figure 8b). There are eight high probability regions, corresponding to the octahedron formed by the six F atoms.

3.5. Self-Diffusion Constants. The self-diffusion coefficient, D, can be calculated by the Einstein relation[16]

$$D = \frac{1}{6}\lim_{t\to\infty}\frac{\mathrm{d}}{\mathrm{d}t}\langle \Delta r(t)^2 \rangle$$

where $\Delta r(t)^2$ is the mean square displacement (MSD) of the center-of-mass of the molecule of interest, and "⟨ ⟩" represents the ensemble average. The long time MSD exhibits a linear behavior with respect to the time t. In this work, the diffusion constant was solved by a linear fitting of the slope in the region from 10 to 50 ps and the values are listed in Table 11. It is found that the diffusion constants of the ions in ionic liquids are on the order of 10^{-11} m^2 s^{-1}, which is 2 orders of magnitude smaller than that of the common small molecules, such as water, at room temperature.

TABLE 11: Self-Diffusion Constant, *D*, of Cations and Anions in Various Ionic Liquids from This Work

		D (10^{-11} m^2 s^{-1})	
RTIL	T (K)	cation	anion
[dmim][PF_6]	400	4.7	3.2
[bmim][PF_6]	298	1.2	1.0
[bmim][PF_6]	313	1.9	1.6
[bmim][PF_6]	333	2.2	1.9
[emim][BF_4]	298	1.1	0.9
[emim][BF_4]	313	1.3	1.2
[bmim][BF_4]	298	1.2	0.8
[dmim]Cl	423	4.8	4.1

4. Conclusions

Room temperature ionic liquids (RTILs) are environment-friendly "green" solvents and have a variety of applications in chemical processes. Understanding of their structure−property relations is of significance in the development of RTILs. Among them, a reasonable force field and its parameters, describing the interactions between molecules and the ions of RTILs, are essential for characterization and simulation of their properties, and furthermore for the design of the target-oriented solvents.

An all-atom force field for 1-alkyl-3-methyl imidazolium family RTILs is developed in the frame of AMBER. Three kinds of refinements are implemented in this work. (1) The force constants of the bonds, angles and torsions are tuned to reproduce the vibrational frequencies. As a result, the frequency of the ring stretching is adjusted from 1808 to 1632 cm^{-1}, which is much closer to the experimental value of 1575 cm^{-1}. (2) The

missing parameters of four dihedral angles in AMBER are obtained by fitting the torsion energy profiles from ab initio (QM) calculations. (3) The VDW diameter for H5 (see Figure 1) is proven requiring further adjustment by the comparisons between the geometries of three ion pairs, which are optimized through the force field and QM calculations.

The force field proposed is validated by liquid phase molecular dynamics simulations for five ionic liquids at different temperatures. Generally, the results are consistent with the previous simulations by other authors. The densities predicted in this work show an improvement over those from other force fields for ionic liquids (see Table 7). The analyses of the components of internal energies show that the system is dominated by electrostatic interactions. In addition, the ionic liquids have extremely high cohesive energy densities and heats of vaporization, corresponding to their very low vapor pressures.

The radial distribution (RDFs) and spatial distribution functions (SDFs) are employed to describe the local structure of these liquids. An evident charge ordering is observed for all the ionic liquids. The site−site RDFs of the hydrogen atoms in cation and the fluorine or chlorine atoms in the anion reveal that the interaction between them is in the order H5 > H4 > H1 > HC and Cl^- > BF_4^- > PF_6^-.

The visualized pictures of the SDFs show intuitively the three-dimensional probability distribution of the atoms of interest around a central ion. There are mainly three regions of the anion distributed around the anion in the first solvation shell.

The self-diffusion coefficients are calculated from the mean square displacement (MSD) of the center-of-mass of the ion. The results indicate that the diffusion coefficients of the ion in ionic liquids are 2 orders of magnitude smaller than that of water at room temperature.

In summary, in this work we propose a force field through refinements and delicate adjustments of main parameters in the frame of AMBER in a systematic way. The force field and its parameters proposed will be applied to the description of the RTILs for the *PVT* relationships, free energies, and other properties. We will report the results in our future work.

Acknowledgment. This work was supported by the National Basic Research Program (No. G2000048010), the National Natural Science Foundation of China (No. 20236010) and the Postdoctoral Scientific Foundation of China (No. 2003033095).

References and Notes

(1) Hagiwara, R.; Ito, Y. *J. Fluorine Chem.* **2000**, *105*, 221.
(2) Blanchard, L. A.; Hancu, D.; Beckman, E. J.; Brennecke, J. F. *Nature* **1999**, *399*, 28.
(3) Tzschucke, C. C.; Markert, C.; Bannwarth, W.; Roller, S.; Hebel, A.; Haag, R. *Angew. Chem., Int. Ed.* **2002**, *41*, 3964.
(4) Welton, T. *Chem. Rev.* **1999**, *99*, 2071.
(5) Dupont, J.; de Souza, R. F.; Suarez, P. A. Z. *Chem. Rev.* **2002**, *102*, 3667.
(6) Ito, Y.; Nohira, T. *Electrochim. Acta* **2000**, *45*, 2611.
(7) de Souza, R. F.; Padilha, J. C.; Goncalves, R. S.; Dupont, J. *Electrochem. Commun.* **2003**, *5*, 728.
(8) Bates, E. D.; Mayton, R. D.; Ntai, I.; James, H. Davis, J. *J. Am. Chem. Soc.* **2002**, *124*, 926.
(9) Zhao, H. *Phys. Chem. Liq.* **2003**, *41*, 545.
(10) Meng, Z.; Dolle, A.; Carper, W. R. *THEOCHEM−J. Mol. Struct.* **2002**, *585*, 119.
(11) Paulechka, Y. U.; Kabo, G. J.; Blokhin, A. V.; Vydrov, O. A.; Magee, J. W.; Frenkel, M. *J. Chem. Eng. Data* **2003**, *48*, 457.
(12) Turner, E. A.; Pye, C. C.; Singer, R. D. *J. Phys. Chem. A* **2003**, *107*, 2277.
(13) Katritzky, A. R.; Lomaka, A.; Petrukhin, R.; Jain, R.; Karelson, M.; Visser, A. E.; Rogers, R. D. *J. Chem. Inf. Comput. Sci.* **2002**, *42*, 71.
(14) Katritzky, A. R.; Jain, R.; Lomaka, A.; Petrukhin, R.; Maran, U.; Karelson, M. *Cryst. Growth Des.* **2001**, *1*, 261.
(15) Dzyuba, S. V.; Bartsch, R. A. *ChemPhysChem* **2002**, *3*, 161.
(16) Frenkel, D.; Smit, B. *Understanding Molecular Simulation*; Academic Press: New York, 1996.
(17) Hanke, C. G.; Price, S. L.; Lynden-Bell, R. M. *Mol. Phys.* **2001**, *99*, 801.
(18) Hanke, C. G.; Atamas, N. A.; Lynden-Bell, R. M. *Green Chem.* **2002**, *4*, 107.
(19) Hanke, C. G.; Johansson, A.; Harper, J. B.; Lynden-Bell, R. M. *Chem. Phys. Lett.* **2003**, *374*, 85.
(20) Hanke, C. G.; Lynden-Bell, R. M. *J. Phys. Chem. B* **2003**, *107*, 10873.
(21) Lynden-Bell, R. M. *Mol. Phys.* **2003**, *101*, 2625.
(22) Lynden-Bell, R. M.; Atamas, N. A.; Vasilyuk, A.; Hanke, C. G. *Mol. Phys.* **2002**, *100*, 3225.
(23) Margulis, C. J.; Stern, H. A.; Berne, B. J. *J. Phys. Chem. B* **2002**, *106*, 12017.
(24) de Andrade, J.; Boes, E. S.; Stassen, H. *J. Phys. Chem. B* **2002**, *106*, 3546.
(25) de Andrade, J.; Boes, E. S.; Stassen, H. *J. Phys. Chem. B* **2002**, *106*, 13344.
(26) Morrow, T. I.; Maginn, E. J. *J. Phys. Chem. B* **2002**, *106*, 12807.
(27) Morrow, T. I.; Maginn, E. J. *J. Phys. Chem. B* **2003**, *107*, 9160.
(28) Chaumont, A.; Engler, E.; Wipff, G. *Inorg. Chem.* **2003**, *42*, 5348.
(29) Chaumont, A.; Wipff, G. *Phys. Chem. Chem. Phys.* **2003**, *5*, 3481.
(30) Shim, Y.; Duan, J. S.; Choi, M. Y.; Kim, H. J. *J. Chem. Phys.* **2003**, *119*, 6411.
(31) Znamenskiy, V.; Kobrak, M. N. *J. Phys. Chem. B* **2004**, *108*, 1072.
(32) Del Popolo, M. G.; Voth, G. A. *J. Phys. Chem. B* **2004**, *108*, 1744.
(33) Lopes, J. N. C.; Deschamps, J.; Padua, A. A. H. *J. Phys. Chem. B* **2004**, *108*, 2038.
(34) Urahata, S. M.; Ribeiro, M. C. C. *J. Chem. Phys.* **2004**, *120*, 1855.
(35) Shah, J. K.; Brennecke, J. F.; Maginn, E. J. *Green Chem.* **2002**, *4*, 112.
(36) Cornell, W. D.; Cieplak, P.; Bayly, C. I.; Gould, I. R.; Merz, K. M.; Ferguson, D. M.; Spellmeyer, D. C.; Fox, T.; Caldwell, J. W.; Kollman, P. A. *J. Am. Chem. Soc.* **1995**, *117*, 5179.
(37) MacKerell, A. D.; Bashford, D.; Bellott, M.; Dunbrack, R. L.; Evanseck, J. D.; Field, M. J.; Fischer, S.; Gao, J.; Guo, H.; Ha, S.; Joseph-McCarthy, D.; Kuchnir, L.; Kuczera, K.; Lau, F. T. K.; Mattos, C.; Michnick, S.; Ngo, T.; Nguyen, D. T.; Prodhom, B.; Reiher, W. E.; Roux, B.; Schlenkrich, M.; Smith, J. C.; Stote, R.; Straub, J.; Watanabe, M.; Wiorkiewicz-Kuczera, J.; Yin, D.; Karplus, M. *J. Phys. Chem. B* **1998**, *102*, 3586.
(38) Jorgensen, W. L.; Maxwell, D. S.; TiradoRives, J. *J. Am. Chem. Soc.* **1996**, *118*, 11225.
(39) Fox, T.; Kollman, P. A. *J. Phys. Chem. B* **1998**, *102*, 8070.
(40) Hardacre, C.; Holbrey, J. D.; McMath, S. E. J.; Bowron, D. T.; Soper, A. K. *J. Chem. Phys.* **2003**, *118*, 273.
(41) Hardacre, C.; McMath, S. E. J.; Nieuwenhuyzen, M.; Bowron, D. T.; Soper, A. K. *J. Phys.-Condes. Matter* **2003**, *15*, S159.
(42) Gu, Z. Y.; Brennecke, J. F. *J. Chem. Eng. Data* **2002**, *47*, 339.
(43) Tosi, M. P.; Fumi, G. *J. Phys. Chem. Solids* **1964**, *25*.
(44) Frisch, M. J.; Trucks, G. W.; Schlegel, H. B.; Scuseria, G. E.; Robb, M. A.; Cheeseman, J. R.; Zakrzewski, V. G.; J. A. Montgomery, J.; Stratmann, R. E.; Burant, J. C.; Dapprich, S.; Millam, J. M.; Daniels, A. D.; Kudin, K. N.; Strain, M. C.; Farkas, O.; Tomasi, J.; Barone, V.; Cossi, M.; Cammi, R.; Mennucci, B.; Pomelli, C.; Adamo, C.; Clifford, S.; Ochterski, J.; Petersson, G. A.; Ayala, P. Y.; Cui, Q.; Morokuma, K.; Malick, D. K.; Rabuck, A. D.; Raghavachari, K.; Foresman, J. B.; Cioslowski, J.; Ortiz, J. V.; Stefanov, B. B.; Liu, G.; Liashenko, A.; Piskorz, P.; Komaromi, I.; Gomperts, R.; Martin, R. L.; Fox, D. J.; Keith, T.; Al-Laham, M. A.; Peng, C. Y.; Nanayakkara, A.; Gonzalez, C.; Challacombe, M.; Gill, P. M. W.; Johnson, B.; Chen, W.; Wong, M. W.; Andres, J. L.; Gonzalez, C.; Head-Gordon, M.; Replogle, E. S.; Pople, J. A. Gaussian 98, Revision A.3. Gaussian, Inc., Pittsburgh, PA, 1998.
(45) Gordon, C. M.; Holbrey, J. D.; Kennedy, A. R.; Seddon, K. R. *J. Mater. Chem.* **1998**, *8*, 2627.
(46) Holbrey, J. D.; Reichert, W. M.; Nieuwenhuyzen, M.; Sheppard, O.; Hardacre, C.; Rogers, R. D. *Chem. Commun.* **2003**, 476.
(47) De Roche, J.; Gordon, C. M.; Imrie, C. T.; Ingram, M. D.; Kennedy, A. R.; Lo Celso, F.; Triolo, A. *Chem. Mater.* **2003**, *15*, 3089.
(48) Xue, H.; Twamley, B.; Shreeve, J. M. *J. Org. Chem.* **2004**, *69*, 1397.
(49) Campbell, J. L. E.; Johnson, K. E.; Torkelson, J. R. *Inorg. Chem.* **1994**, *33*, 3340.
(50) Takahashi, S.; Curtiss, L. A.; Gosztola, D.; Koura, N.; Saboungi, M. L. *Inorg. Chem.* **1995**, *34*, 2990.
(51) Lii, J. H.; Allinger, N. L. *J. Am. Chem. Soc.* **1989**, *111*, 8566.
(52) Pappu, R. V.; Hart, R. K.; Ponder, J. W. *J. Phys. Chem. B* **1998**, *102*, 9725.
(53) Wang, J. M.; Kollman, P. A. *J. Comput. Chem.* **2001**, *22*, 1219.
(54) Bayly, C. I.; Cieplak, P.; Cornell, W. D.; Kollman, P. A. *J. Phys. Chem.* **1993**, *97*, 10269.

(55) Cornell, W. D.; Cieplak, P.; Bayly, C. I.; Kollman, P. A. *J. Am. Chem. Soc.* **1993**, *115*, 9620.
(56) Cieplak, P.; Cornell, W. D.; Bayly, C.; Kollman, P. A. *J. Comput. Chem.* **1995**, *16*, 1357.
(57) Wang, J. M.; Cieplak, P.; Kollman, P. A. *J. Comput. Chem.* **2000**, *21*, 1049.
(58) Chalasinski, G.; Szczesniak, M. M. *Chem. Rev.* **2000**, *100*, 4227.
(59) Engkvist, O.; Astrand, P. O.; Karlstrom, G. *Chem. Rev.* **2000**, *100*, 4087.
(60) Chen, I. J.; Yin, D. X.; MacKerell, A. D. *J. Comput. Chem.* **2002**, *23*, 199.
(61) McDonald, N. A.; Jorgensen, W. L. *J. Phys. Chem. B* **1998**, *102*, 8049.
(62) Fuller, J.; Carlin, R. T.; Delong, H. C.; Haworth, D. *J. Chem. Soc., Chem. Commun.* **1994**, 299.
(63) Lyubartsev, A. P.; Laaksonen, A. *Comput. Phys. Commun.* **2000**, *128*, 565.
(64) Martyna, G. J.; Tuckerman, M. E.; Tobias, D. J.; Klein, M. L. *Mol. Phys.* **1996**, 8*7*, 1117.
(65) Tuckerman, M.; Berne, B. J.; Martyna, G. J. *J. Chem. Phys.* **1992**, 9*7*, 1990.
(66) Deleeuw, S. W.; Perram, J. W.; Smith, E. R. *Proc. R. Soc. London, Ser. A: Math. Phys. Eng. Sci.* **1983**, *388*, 177.
(67) Wang, J. J.; Tian, Y.; Zhao, Y.; Zhuo, K. *Green Chem.* **2003**, *5*, 618.
(68) Headley, A. D.; Jackson, N. M. *J. Phys. Org. Chem.* **2002**, 15, 52.
(69) Wasserscheid, P.; Keim, W. *Angew. Chem., Int. Ed.* **2000**, 39, 3773.
(70) Wilkes, J. S.; Zaworotko, M. J. *J. Chem. Soc.,Chem. Commun.* **1992**, 965.
(71) Holbrey, J. D.; Seddon, K. R. *J. Chem. Soc., Dalton Trans.* **1999**, 2133.
(72) Huang, J. F.; Chen, P. Y.; Sun, I. W.; Wang, S. P. *Inorg. Chim. Acta* **2001**, 3*20*, 7.
(73) Laaksonen, L. *J. Mol. Graphics* **1992**, 1*0*, 33.
(74) Yoshida, Y.; Muroi, K.; Otsuka, A.; Saito, G.; Takahashi, M.; Yoko, T. *Inorg. Chem.* **2004**, *43*, 1458.
(75) Matsumoto, K.; Tsuda, T.; Hagiwara, R.; Ito, Y.; Tamada, O. *Solid State Sci.* **2002**, *4*, 23.
(76) Holbrey, J. D.; Reichert, W. M.; Nieuwenhuyzen, M.; Johnston, S.; Seddon, K. R.; Rogers, R. D. *Chem. Commun.* **2003**, 1636.
(77) van den Broeke, J.; Stam, M.; Lutz, M.; Kooijman, H.; Spek, A. L.; Deelman, B. J.; van Koten, G. *Eur. J. Inorg. Chem.* **2003**, 2798.
(78) Downard, A.; Earle, M. J.; Hardacre, C.; McMath, S. E. J.; Nieuwenhuyzen, M.; Teat, S. J. *Chem. Mater.* **2004**, *16*, 43.
(79) Noda, A.; Hayamizu, K.; Watanabe, M. *J. Phys. Chem. B* **2001**, *105*, 4603.
(80) Fannin, A. A.; Floreani, D. A.; King, L. A.; Landers, J. S.; Piersma, B. J.; Stech, D. J.; Vaughn, R. L.; Wilkes, J. S.; Williams, J. L. *J. Phys. Chem.* **1984**, *88*, 2614.